Energy Materials

Supplementary Materials

Corrosion-induced surface reconstruction enhances $RuO_2/NiFe(OH)_x$ for efficient hydrogen evolution reaction

Chenxing Mao[1,#], Chang Zhang[2,#], Jie Chen[3], Junpo Guo[3,*], Zhifei Cui[1], Rongtao Zhang[1], Xin Li[1], Rui Li[4], Yinan Liu[4,*], Xupo Liu[1,3,*]

[1]Henan Engineering Research Center of Design and Recycle for Advanced Electrochemical Energy Storage Materials, School of Materials Science and Engineering, Henan Normal University, Xinxiang 453007, Henan, China.

[2]School of Materials Science and Engineering, Huazhong University of Science and Technology, Wuhan 430074, Hubei, China.

[3]School of Chemistry and Chemical Engineering, Henan Normal University, Xinxiang 453007, Henan, China.

[4]Joint Key Laboratory of the Ministry of Education, Institute of Applied Physics and Materials Engineering, University of Macau, Macao 999078, China.

[#]These authors contributed equally to this work.

[*]**Correspondence to:** Dr. Junpo Guo, School of Chemistry and Chemical Engineering, Henan Normal University, Xinxiang 453007, Henan, China. E-mail: guojunpo@htu.edu.cn; Dr. Yinan Liu, Joint Key Laboratory of the Ministry of Education, Institute of Applied Physics and Materials Engineering, University of Macau, Macao 999078, China. E-mail: yc27809@um.edu.mo; Prof. Xupo Liu, Henan Engineering Research Center of Design and Recycle for Advanced Electrochemical Energy Storage Materials, School of Materials Science and Engineering, Henan Normal University, Xinxiang 453007, Henan, China. E-mail: liuxupo@htu.edu.cn

Supplementary Table 1. Summary of experimental instrument information

Instrument/equipment	Model/specification	Manufacturer
Analytical balance	CP214	OHAUS Corporation, Parsippany, NJ, USA
Laboratory ultrapure water purification system	KQ-100KDB	Hangzhou Yijie Technology Co., Ltd. (EJER), Hangzhou, China
Magnetic stirrer	S10-3	Shanghai Sile Instrument Co., Ltd., Shanghai, China
Ultrasonic cleaner	KQ5200DE	Kunshan Ultrasonic Instruments Co., Ltd. (Shumei), Kunshan, China
Forced-air drying oven	DHG-9030	Shanghai Yiheng Instrument Co., Ltd., Shanghai, China
Scanning electron microscope (SEM)	Sirion 200	FEI Company, Hillsboro, OR, USA
X-ray diffractometer (XRD)	X'Pert^3 Powder	PANalytical B.V., Almelo, the Netherlands
Electron energy-loss spectrometer (EELS)	Enfina	Gatan, Inc., Pleasanton, CA, USA
Transmission electron microscope (TEM)	Talos F200X	Thermo Fisher Scientific, Waltham, MA, USA
X-ray photoelectron spectrometer (XPS)	ESCALAB 250Xi	Thermo Fisher Scientific, Waltham, MA, USA
Electrochemical workstation	CHI660E	Shanghai Chenhua Instrument Co., Ltd., Shanghai, China
Graphite electrode	5 mm diameter	Tianjin Aida Hengsheng Technology Co., Ltd., Tianjin, China

Platinum sheet electrode holder/clamp	Pt210	Tianjin Aida Hengsheng Technology Co., Ltd., Tianjin, China
Hg/HgO reference electrode	R0501	Tianjin Aida Hengsheng Technology Co., Ltd., Tianjin, China
Saturated calomel electrode (SCE)	R0232	Tianjin Aida Hengsheng Technology Co., Ltd., Tianjin, China

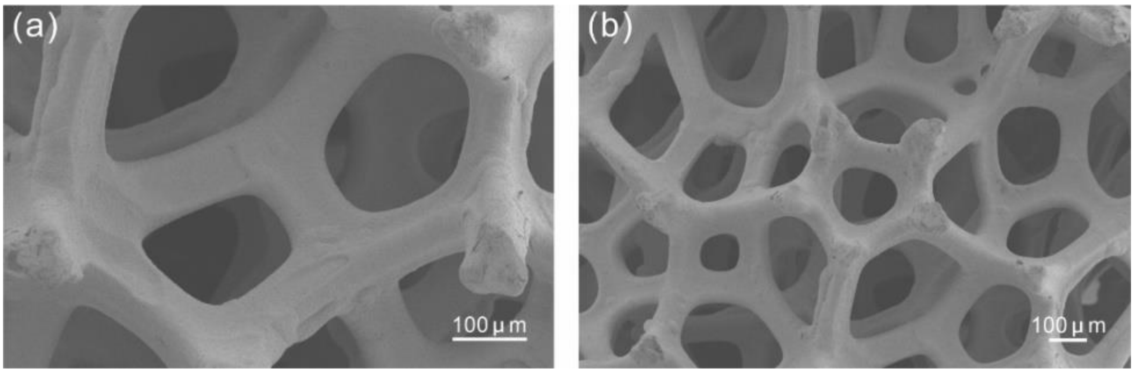

Supplementary Figure 1. (a-b) SEM images of NFF.

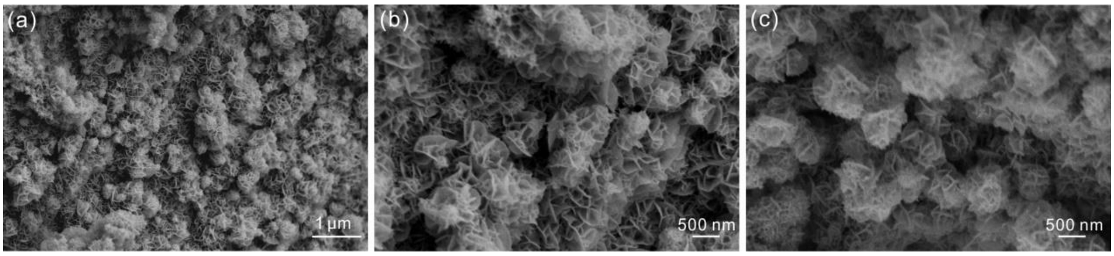

Supplementary Figure 2. (a-b) SEM images of $NiFe(OH)_x$. (c) SEM image of $RuO_2/NiFe(OH)_x$.

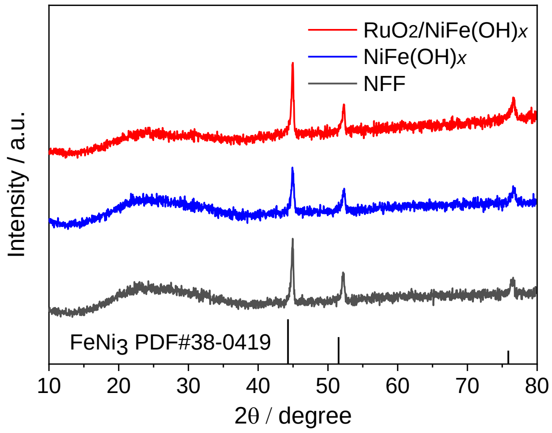

Supplementary Figure 3. XRD patterns of NFF, NiFe(OH)$_x$ and RuO$_2$/NiFe(OH)$_x$.

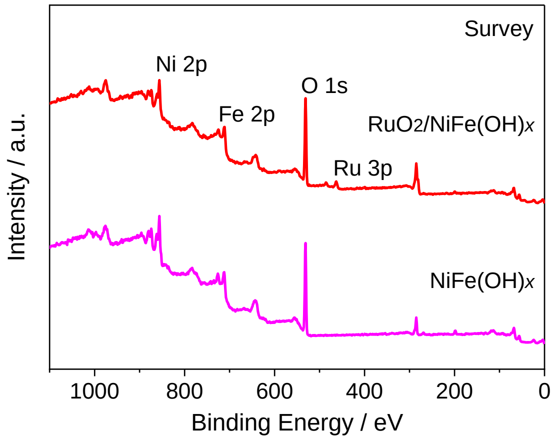

Supplementary Figure 4. XPS survey spectra of NiFe(OH)$_x$ and RuO$_2$/NiFe(OH)$_x$.

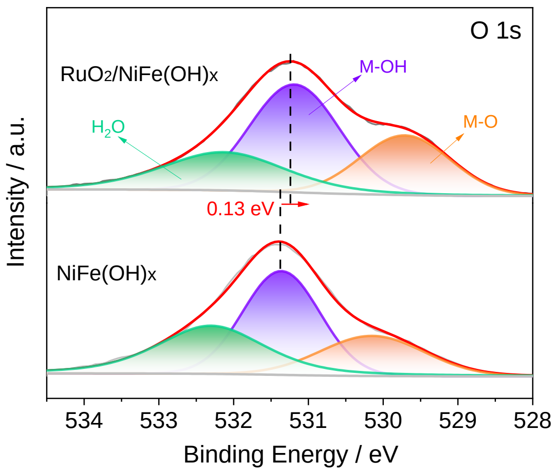

Supplementary Figure 5. High resolution XPS spectra of O 1s regions.

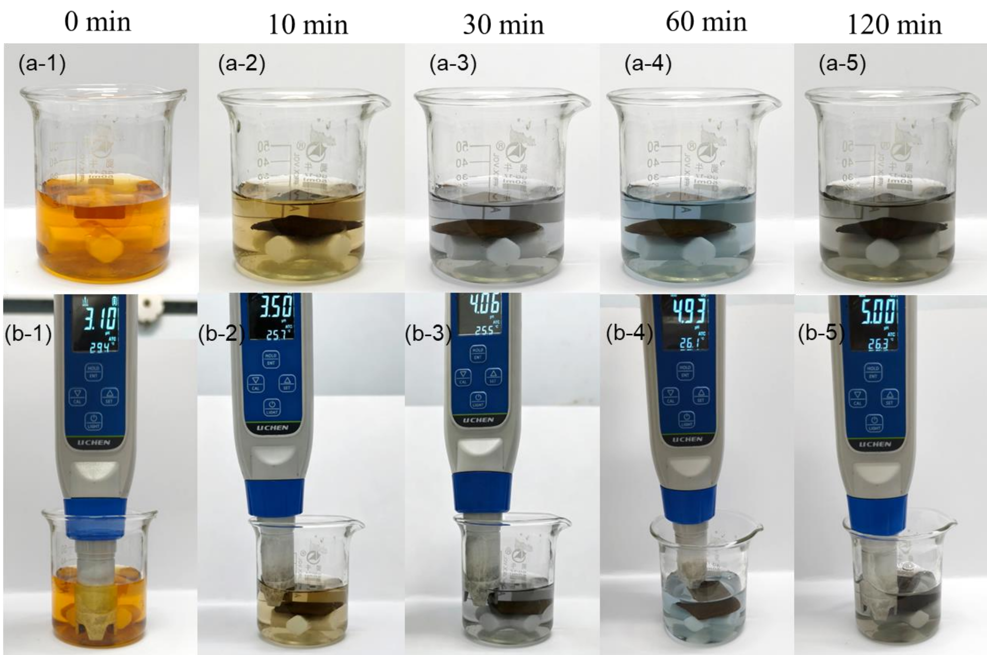

Supplementary Figure 6. (a) Color changes and (b) pH evolution of the $RuCl_3$ solution during $NiFe(OH)_x$ immersion.

Supplementary Table 2. Time-dependent pH changes of the $RuCl_3$ solution during the immersion process of the $NiFe(OH)_x$ electrode.

Immersion time/min	pH value	Immersion time/min	pH value
0	3.10	60	4.93
10	3.50	120	5.00
30	4.06		

Supplementary Table 3. ICP-OES results of $RuCl_3$ solution before and after the $NiFe(OH)_x$ immersion

Condition	Ni/mg L^{-1}	Fe/mg L^{-1}	Ru/mg L^{-1}
Before immersion	0.0949	0.3047	145.7364
After immersion	68.1262	210.2132	19.9406

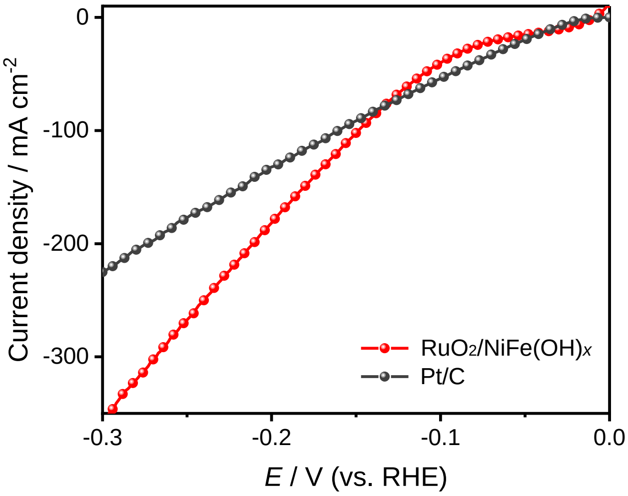

Supplementary Figure 7. HER polarization curves of $RuO_2/NiFe(OH)_x$ and commercial Pt/C in 1.0 M KOH.

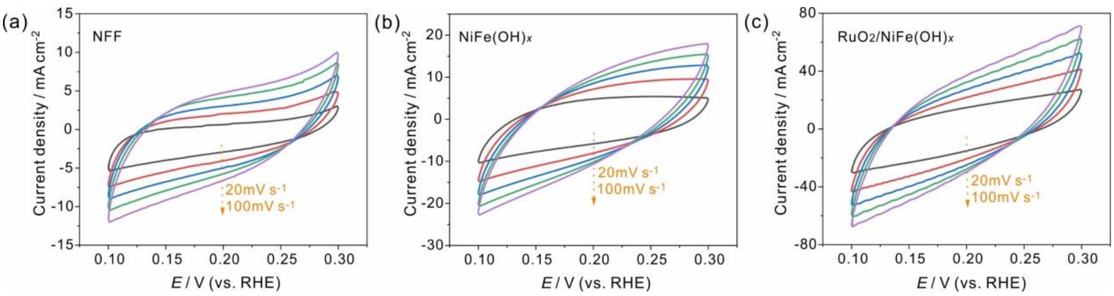

Supplementary Figure 8. CV curves of (a) NFF, (b) $NiFe(OH)_x$ and (c) $RuO_2/NiFe(OH)_x$ at the different scanning rates.

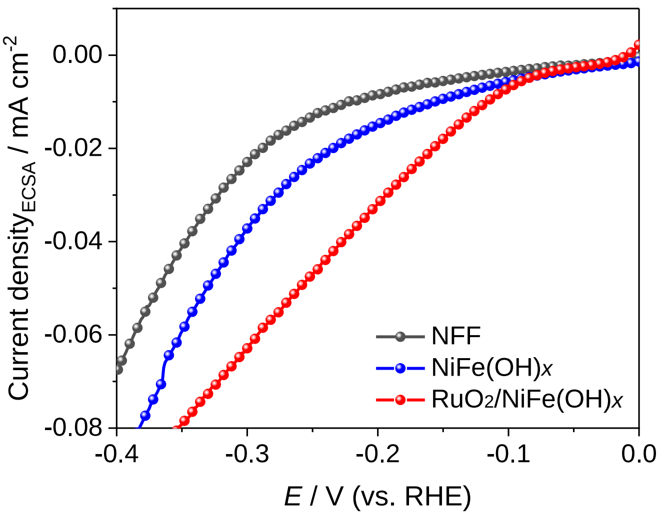

Supplementary Figure 9. ECSA-normalized HER polarization curves of NFF, $NiFe(OH)_x$ and $RuO_2/NiFe(OH)_x$.

Supplementary Table 4. Comparison of the HER performances of $RuO_2/NiFe(OH)_x$ with the recently reported electrocatalysts

Sample	Overpotentials at 100 mA cm^{-2} (mV)	Tafel slopes (mV dec^{-1})	Stability test	References
$RuO_2/NiFe(OH)_x$	149	33.70	200 mA cm^{-2} for 100h	This work
AC-Ni/NF	153	46.8	10 mA cm^{-2} for 24h	[1]
$SnFeS_xO_y/NF$	167	90	50 mA cm^{-2} for 54h	[2]
Ni/NM	178	89	100 mA cm^{-2} for 72h	[3]
CoFe-P/NF-1	180	84	50 mA cm^{-2} for 25h	[4]
$CoNi_2S_4$@NiMn LDH/SCC	184	97.8	20 and 100 mA cm^{-2} for 12h	[5]
CoNi-LDH/Co@NC	187	94	50 and 100 mA cm^{-2} for 20h	[6]
NiSe@NiFe-LDH/NF	193	74.3	195mV for 100h	[7]
$NiFeO_xH_y/Ni_3Fe$	196	111	10 mA cm^{-2} for 2h	[8]
$NiCo_{(nf)}$-P	199	112	500 and 1000 mA cm^{-2} for 30h	[9]
CdS@NiCo-LDH	202	41.3	100 mA cm^{-2} for 30h	[10]
$NiAl-LDH/Ni_3S_2/NF$	209.2	68.7	20 mV for 5h	[11]

Pt/Ni(OH)2/NF-A	211	37.6	20 mV for 20h	[12]
Mn–Co (7.5)/GP	216	121	100mV for 24h	[13]
Mo-doped CoFe LDH/NF	227	94	100 mA cm^{-2} for 24h	[14]
CNS/LDH/NF	228	65	10 mA cm^{-2} for 14h	[15]
$Fe_{0.25}Co_{0.75}$	245	127	100 mA cm^{-2} for 100h	[16]
Co_3S_4@NiCo-LDH/NF	251	121.6	131.5 and 251 mV for 100h	[17]
$Co(OH)_2$/Ni-Co-S-8h	254	88	20 mA cm^{-2} for 14h	[18]
$LiTiPO_4F$/NF	290	48	290 mV for 57h	[19]

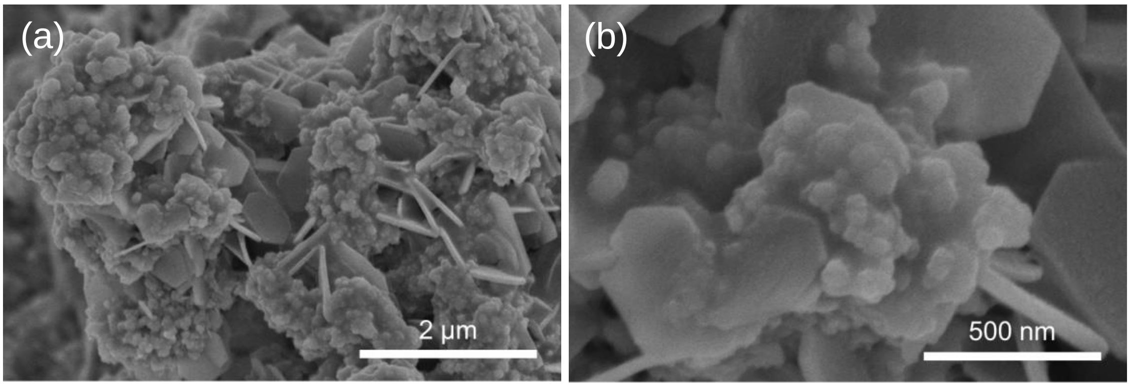

Supplementary Figure 10. (a-b) SEM images of $RuO_2/NiFe(OH)_x$ after the stability test.

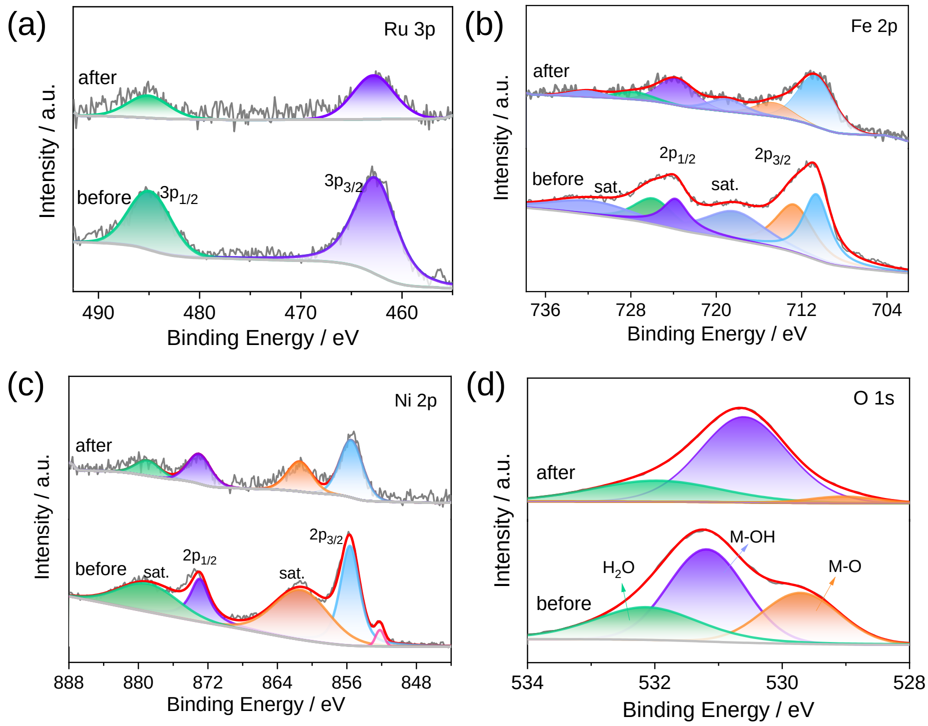

Supplementary Figure 11. XPS spectra of $RuO_2/NiFe(OH)_x$ before and after the stability test: (a) Ru 3p, (b) Fe 2p, (c) Ni 2p, and (d) O 1s..

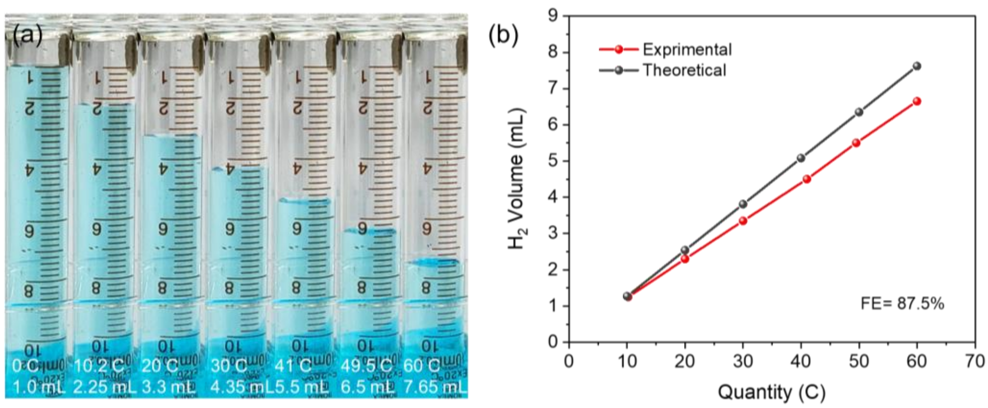

Supplementary Figure 12. Faradaic efficiency measurement of $RuO_2/NiFe(OH)_x$ for hydrogen generation. (a) Photographs of the collected H_2 gas at different electrolysis times. (b) Comparison between the experimentally measured and theoretically calculated H_2 volumes during HER.

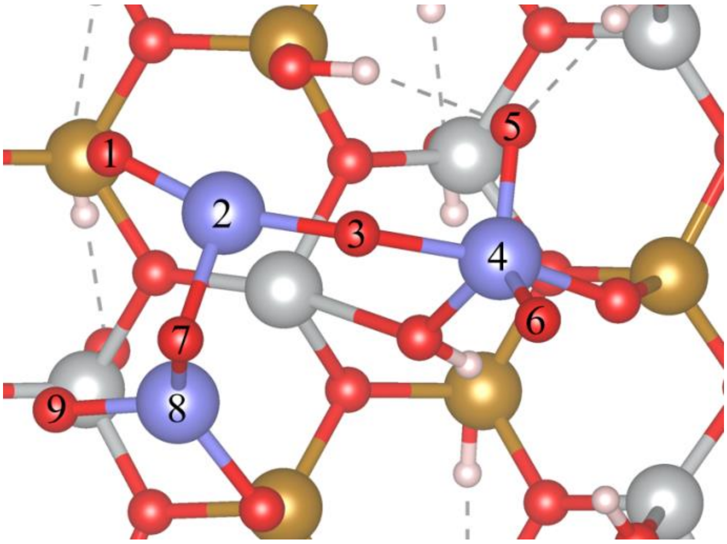

Supplementary Figure 13. Optimized model (position-I) with labeled atoms for Bader charge analysis.

Supplementary Table 5. Bader charges of labeled atoms in optimized model (position-I)

Site	**1**	**2**	**3**	**4**	**5**	**6**	**7**	**8**	**9**
Charge	-0.833	1.929	-0.97	2.64	-0.912	-0.803	-0.92	1.868	-0.803
Total	1.196								

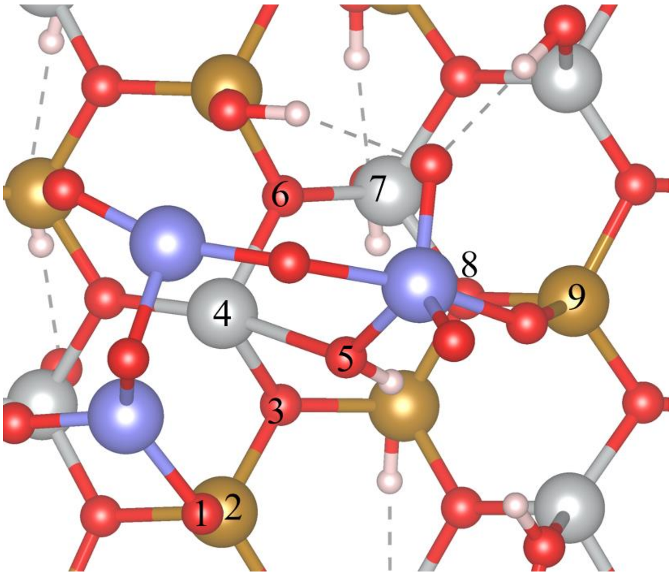

Supplementary Figure 14. Optimized model (position-II) with labeled atoms for Bader charge analysis.

Supplementary Table 6. Bader charges of labeled atoms in optimized model (position-II)

Site	**1**	**2**	**3**	**4**	**5**	**6**	**7**	**8**	**9**
Charge	-1.042	1.719	-1.097	1.048	-1.153	-1.049	1.265	-1.122	1.766

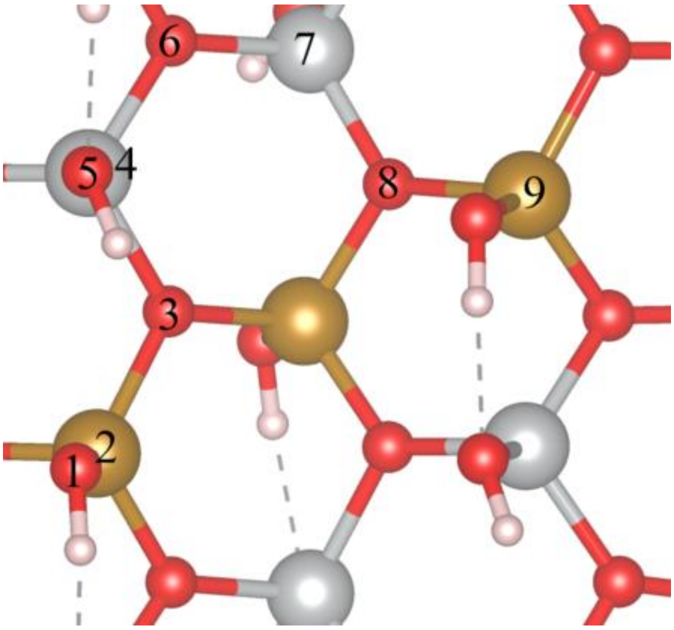

Supplementary Figure 15. Optimized model (position-III) with labeled atoms for Bader charge analysis.

Supplementary Table 7. Bader charges of labeled atoms in optimized model (position-III)

Site	**1**	**2**	**3**	**4**	**5**	**6**	**7**	**8**	**9**
Charge	-1.11	1.794	-1.118	1.308	-1.116	-1.058	1.319	-1.018	1.772

Supplementary Table 8. Comparison of water-splitting performances of the $NiFe(OH)_x$ ‖ RuO_2/ $NiFe(OH)_x$ system with the recently reported devices

HER catalyst	OER catalyst	Cell voltage at 100 mA cm^{-2} (V)	Stability test	References
$RuO_2/NiFe(OH)_x$	$NiFe(OH)_x$	1.656	100 and 200 mA cm^{-2} for 100h	This work
IrNi PMAN	IrNi PMAN	1.69	50 mA cm^{-2} for 24h	[20]
$CoNi_2S_4$@NiMn LDH/SCC	$CoNi_2S_4$@NiMn LDH/SCC	1.691	50 mA cm^{-2} for 12h	[5]
Pt/C	np-CFO(Al and Mn)	1.70	500 mA cm^{-2} for 100 h	[21]
NF10	NF10	1.703	100 and 400 mA cm^{-2} for 105h	[22]
NiSe@NiFe-LDH /NF	NiSe@NiFe-LDH/ NF	1.705	1.65 and 1.71 V for 100h	[7]
H-NMO/CMO/CF-450	H-NMO/CMO/CF-450	1.71	100 mA cm^{-2} for 300h	[23]
NiCo(nf)- P	NiCo(nf)- P	1.74	500 and 1000 mA cm^{-2} for 30h	[9]
NiCoP/NF	F-NC2AL@ZFAL/ NF	1.75	100 mA cm^{-2} for 22 h	[24]

Ni/NM	NiFe-LDH/Ni/NM	1.80	500 and 1000 mA cm^{-2} for 154h	[3]
$NiMoO_4$-S/Ni_3S_2/NF	$NiMoO_4$-S/Ni_3S_2/NF	1.85	1.52 and 1.85 V for 70 h	[25]
MNF-2	MNF-2	1.90	100 mA cm^{-2} for 50 h	[26]
(Mo/Co)O_x–Cu@NF	(Mo/Co)O_x–Cu@NF	1.99	10 mA cm^{-2} for 24 h	[27]

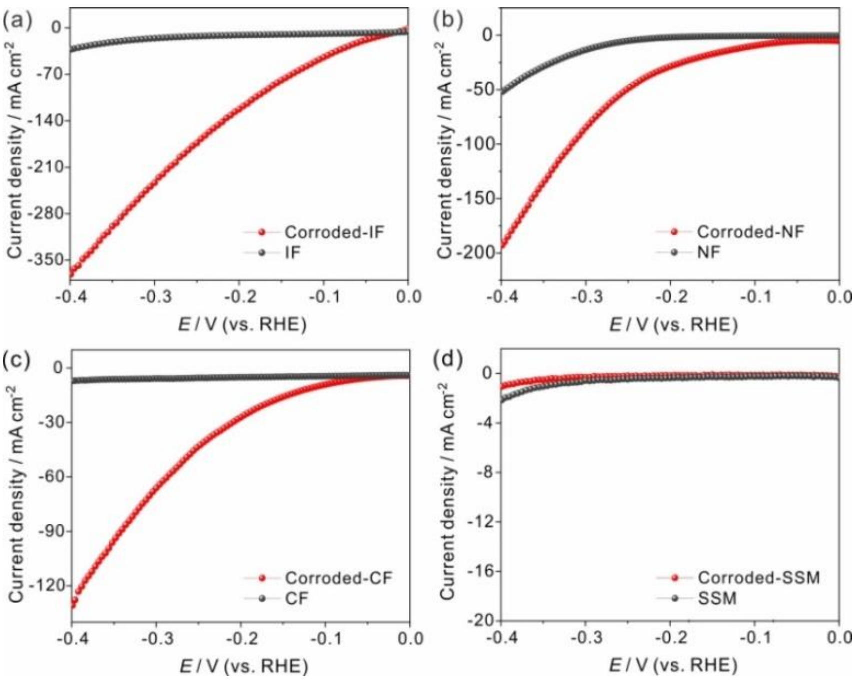

Supplementary Figure 16. Comparison of the HER polarization curves of (a) IF, (b) NF, (c) CF and (d) SSM before and after corrosion.

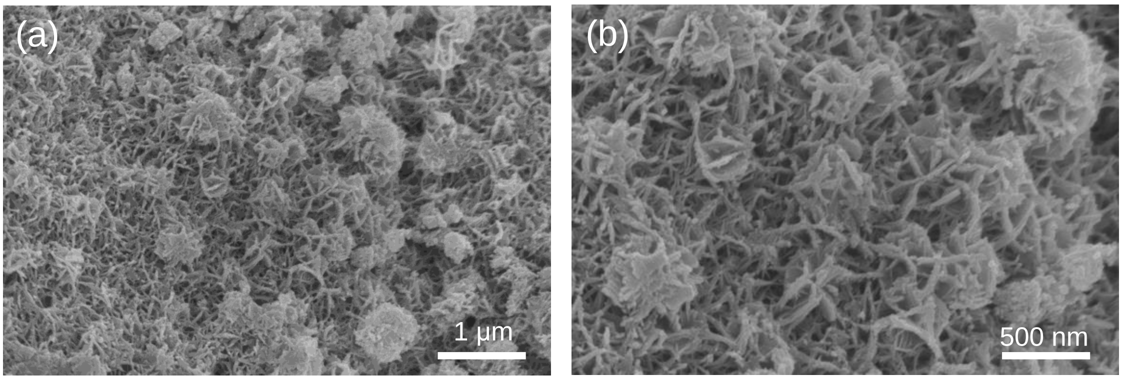

Supplementary Figure 17. (a-b) SEM images of large-size $RuO_2/NiFe(OH)_x$ electrode.

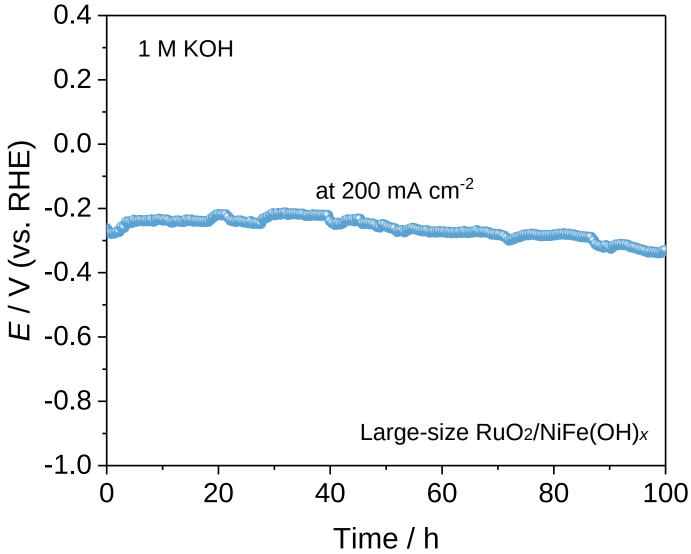

Supplementary Figure 18. Chronopotentiometry curve of the large-size $RuO_2/NiFe(OH)_x$ electrode at the constant current density of 200 mA cm^{-2}.

REFERENCES

1. Lai, W.; Ge, L.; Li, H.; et al. In situ Raman spectroscopic study towards the growth and excellent HER catalysis of Ni/Ni$(OH)_2$ heterostructure. *Int. J. Hydrogen Energy* **2021,** *46*, 26861-26872. DOI: 10.1016/j.ijhydene.2021.05.158
2. Zhang, T.; Han, J. Y.; Tang, T. M.; Sun, J. R.; Guan, J. Q. Binder-free bifunctional SnFe sulfide/oxyhydroxide heterostructure electrocatalysts for overall water splitting. *Int. J. Hydrogen Energy* **2023,** *48*, 4594-4602. DOI: 10.1016/j.ijhydene.2022.11.039
3. Zhou, H.; Wang, H. L.; Lai, C. G.; et al. Hierarchical heterogeneous NiFe-LDH/Ni/NM nanosheets grown in situ for stably overall water splitting at large current densities. *J. Electroanal. Chem.* **2022,** *919*, 116527. DOI: 10.1016/j.jelechem.2022.116527
4. Wang, X.; Wang, C.; Lai, F.; Sun, H.; Yu, N.; Geng, B. Self-supported CoFe-P nanosheets as a bifunctional catalyst for overall water splitting. *ACS Appl. Nano Mater.* **2021,** *4*, 12083-12090. DOI: 10.1021/acsanm.1c02607
5. Wang, P.; Qi, J.; Li, C.; Li, W.; Wang, T.; Liang, C. Hierarchical $CoNi_2S_4$@NiMn-layered double hydroxide heterostructure nanoarrays on superhydrophilic carbon cloth for enhanced overall water splitting. *Electrochim. Acta* **2020,** *345*, 136247. DOI: 10.1016/j.electacta.2020.136247
6. Sang, Y.; Guo, Z. X.; Li, G. H.; Xue, Y. Y.; Xue, J. W. Enhanced water electrolysis activity by CoNi-LDH/Co -nitrogen-doped carbon heterostructure with dual catalytic active sites. *Electrochim. Acta* **2023,** *444*, 141956. DOI: 10.1016/j.electacta.2023.141956
7. Pan, Z. Y.; Tang, Z.; Yaseen, M.; Zhan, Y. Z. NiSe and Fe-based layerd double hydroxide nanosheet/Ni foam bifunctional catalyst for water splitting. *ACS Appl. Nano Mater.* **2022,** *5*, 16793-16803. DOI: 10.1021/acsanm.2c03764
8. Baibars, I. O.; Abd El-Moghny, M. G.; El-Deab, M. S. $NiFeO_xH_y/Ni_3Fe$ interface design via electropassivation for superior catalysis of HER. *J. Environ. Chem. Eng.* **2022,** *10*, 108736. DOI: 10.1016/j.jece.2022.108736
9. Xu, Z. C.; Yeh, C. L.; Chen, J. L.; Lin, J. T.; Ho, K. C.; Lin, R. Y. Y.

Metal-organic framework-derived 2D NiCoP nanoflakes from layered double hydroxide nanosheets for efficient electrocatalytic water splitting at high current densities. *ACS Sustainable Chem. Eng.* **2022,** *10*, 11577-11586. DOI: 10.1021/acssuschemeng.2c03250
10. Pirkarami, A.; Rasouli, S.; Ghasemi, E. 3-D CdS@NiCo layered double hydroxide core-shell photoelectrocatalyst used for efficient overall water splitting. *Appl. Catal. B Environ.* **2019,** *241*, 28-40. DOI: 10.1016/j.apcatb.2018.09.021
11. Zhao, L.; Guo, Z. A.; Liu, Z. F. Facile synthesis and efficient electrochemical water splitting of bifunctional nanostructured Ni-based layered double hydroxide/sulfide composite. *J. Alloys Compd.* **2022,** *910*, 164880. DOI: 10.1016/j.jallcom.2022.164880
12. Gu, Y.; Wang, Y.; Shi, J.; et al. Well-dispersed Pt nanodots interfaced with $Ni(OH)_2$ on anodized nickel foam for efficient hydrogen evolution reaction. *Int. J. Hydrogen Energy* **2020,** *45*, 27067-27077. DOI: 10.1016/j.ijhydene.2020.07.047
13. Shamloofard, M.; Shahrokhian, S. Morphology modulation and phase transformation of manganese-cobalt carbonate hydroxide caused by fluoride doping and its effect on boosting the overall water electrolysis. *Inorg. Chem.* **2023,** *62*, 1178-1191. DOI: 10.1021/acs.inorgchem.2c03529
14. Zhao, G.; Wang, B.; Yan, Q.; Xia, X. Mo-doping-assisted electrochemical transformation to generate CoFe LDH as the highly efficient electrocatalyst for overall water splitting. *J. Alloys Compd.* **2022,** *902*, 163738. DOI: 10.1016/j.jallcom.2022.163738
15. Zhang, W. L.; Wang, S.; Wang, Z. S.; Cao, G. X.; Zhang, P.; Liu, C. Constructing the heterostructure of sulfide and layered double hydroxide as bifunctional electrocatalyst for overall water splitting. *J. Solid State Electrochem.* **2023,** *27*, 575-583. DOI: 10.1007/s10008-022-05350-4
16. Walendzik, I.; Kordek-Khalil, K.; Rutkowski, P. Quick-to-synthesize hybrid electrodes composed of activated carbon cloth with Co/Fe-based films as bifunctional electrocatalysts for water splitting. *Int. J. Hydrogen Energy* **2023,** *48*, 25741-25754. DOI: 10.1016/j.ijhydene.2023.03.092

17. Xu, X. H.; Su, L.; Zhang, Y. J.; Dong, L. J.; Miao, X. Y. Hierarchical tube brush-like Co_3S_4@NiCo-LDH on Ni foam as a bifunctional electrocatalyst for overall water splitting. *New J. Chem.* **2021,** *45*, 15429-15436. DOI: 10.1039/d1nj02093e
18. Wu, F.; Guo, X. X.; Hao, G. Z.; Hu, Y. B.; Jiang, W. Self-supported hollow $Co(OH)_2$/NiCo sulfide hybrid nanotube arrays as efficient electrocatalysts for overall water splitting. *J. Solid State Electrochem.* **2019,** *23*, 2627-2637. DOI: 10.1007/s10008-019-04362-x
19. Srinivasa, N.; Rangaswamy, P.; Yogeeshwari, R. T.; Manjunatha, C.; Ashoka, S. Mesoporous $LiTiPO_4F$ nanoparticles: a new stable and high performance bifunctional electrocatalyst for electrochemical water splitting. *Surf. Interfaces* **2021,** *25*, 101188. DOI: 10.1016/j.surfin.2021.101188
20. Zhou, Z.-H.; Li, W.-H.; Zhang, Z.; Zhao, X.-C.; Cao, W.; Huang, Q.-S. Ni optimizes Ir reaction pathway through IrNi alloy synergistic effect to improve overall water splitting efficiency. *Int. J. Hydrogen Energy* **2023,** *48*, 8440-8449. DOI: 10.1016/j.ijhydene.2022.11.178
21. Shen, H.; Du, H.; Li, P.; Wang, M. Hierarchical flaky spinel structure with Al and Mn Co-doping towards preferable oxygen evolution performance. *Materials* **2025,** *18, 3633*. DOI: 10.3390/ma18153633
22. Chen, Y.-F.; Li, J.-H.; Liu, T.-T.; et al. Constructing robust NiFe LDHs-NiFe alloy gradient hybrid bifunctional catalyst for overall water splitting: one-step electrodeposition and surface reconstruction. *Rare Met.* **2023,** *42*, 2272-2283. DOI: 10.1007/s12598-022-02249-x
23. Gao, Y.; Ding, H.; Fan, X.; Xiao, J.; Zhang, L.; Xu, G. Anchoring cobalt molybdenum nickel alloy nanoparticles on molybdenum dioxide nanosheets as efficient and stable self-supported catalyst for overall water splitting at high current density. *J. Colloid Interface Sci.* **2023,** *648*, 745-754. DOI: 10.1016/j.jcis.2023.06.053
24. Hou, Z.; Zhu, Y.; Du, W.; Jia, X.; Huang, T.; Huang, K.-J. Nano-control synthesis the porous network of NiCoP and F doped $NiCo_2Al$-LDHs@ZnFeAl-LDHs nanosheets as superior catalyst for efficient overall water splitting. *J. Ind. Eng. Chem.* **2022,** *112*, 85-95. DOI: 10.1016/j.jiec.2022.05.002

25. Zhang, T.; Xu, D.; Liu, P.; et al. Constructing defect-rich S-doped $NiMoO_4/Ni_3S_2$ 2D/2D heterostructures as highly efficient and stable bifunctional electrocatalysts for overall water splitting. *J. Alloys Compd.* **2024,** *970*, 172530. DOI: 10.1016/j.jallcom.2023.172530
26. Gultom, N. S.; Chen, T.-S.; Silitonga, M. Z.; Kuo, D.-H. Overall water splitting realized by overall sputtering thin-film technology for a bifunctional MoNiFe electrode: a green technology for green hydrogen. *Appl. Catal. B Environ.* **2023,** *322*, 122103. DOI: 10.1016/j.apcatb.2022.122103
27. Tartour, A. R.; Sanad, M. M. S.; El-Hallag, I. S.; Moharram, Y. I. Novel mixed heterovalent (Mo/Co)O_x-zerovalent Cu system as bi-functional electrocatalyst for overall water splitting. *Sci. Rep.* **2024,** *14, 4601*. DOI: 10.1038/s41598-024-54934-9